Moiré-pattern interlayer potentials in van der Waals materials in the random-phase approximation

Nicolas Leconte,[1] Jeil Jung,[1,*] Sébastien Lebègue,[2] and Tim Gould[3]
[1]*Department of Physics, University of Seoul, Seoul 02504, Korea*
[2]*Laboratoire de Cristallographie, Résonance Magnétique et Modélisations (CRM2, UMR CNRS 7036), Institut Jean Barriol, Université de Lorraine, BP 239, Boulevard des Aiguillettes, 54506 Vandoeuvre-lès-Nancy, France*
[3]*Qld Micro- and Nanotechnology Centre, Griffith University, Nathan, Qld 4111, Australia*
(Received 3 September 2017; published 27 November 2017)

Stacking-dependent interlayer interactions are important for understanding the structural and electronic properties in incommensurable two-dimensional material assemblies where long-range moiré patterns arise due to small lattice constant mismatch or twist angles. Here we study the stacking-dependent interlayer coupling energies between graphene (G) and hexagonal boron nitride (BN) homo- and heterostructures using high-level random-phase approximation (RPA) *ab initio* calculations. Our results show that although total binding energies within LDA and RPA differ substantially by a factor of 200%–400%, the energy differences as a function of stacking configuration yield nearly constant values with variations smaller than 20%, meaning that LDA estimates are quite reliable. We produce phenomenological fits to these energy differences, which allows us to calculate various properties of interest including interlayer spacing, sliding energetics, pressure gradients, and elastic coefficients to high accuracy. The importance of long-range interactions (captured by RPA but not LDA) on various properties is also discussed. Parametrizations for all fits are provided.

DOI: 10.1103/PhysRevB.96.195431

I. INTRODUCTION

The quest for new artificial materials by assembling atomically thin two-dimensional van der Waals materials [1–3] has seen a new surge of interest during the last decade since the seminal transport experiments on graphene [4–6]. Artificial layered materials often form incommensurable crystals due to finite twist angles or differences in the lattice constants which leads to moiré patterns that dictate the appearance of a superlattice on top of the constituent crystal lattices. These moiré patterns that form at the interface of incommensurable crystals lead to important features in the electronic structure of graphene at energy regions accessible by gate doping for sufficiently long moiré periods [7,8] opening up new possibilities of tailoring electronic properties through the control of interface superlattices. At the same time, non-negligible effects of moiré strains that reconfigure the stacking arrangement of the lattices in the limit of long moiré periods have been observed through tunneling electron microscopy [9,10], and atomic force microscopy [11], rationalized by the quadratic decrease of the elastic energy with the moiré period [12]. Because the atomic and electronic structure of incommensurable moiré patterned systems can be described as a collection of commensurate crystals with varying stacking configurations [13], an important first step towards understanding the physics of the moiré patterns is to understand the stacking dependent interlayer coupling between commensurate vertical heterolayer systems with short crystalline periods.

Two important examples of atomically thin van der Waals materials are graphene [14–17], a single-atom thick sheet of carbon atoms arranged in a honeycomb lattice, and hexagonal boron nitride (BN) sheets [18], whose honeycomb lattice consist of alternating boron and nitrogen atoms. Graphene is a zero band gap semimetal near charge neutrality that obeys a Dirac-like dispersion, whereas BN is a wide band gap insulator with an experimental bulk band gap of 5.8 eV [19,20]. Hexagonal boron nitride has been highlighted as an excellent dielectric barrier material in field effect transistors with improved device mobilities through elimination of extrinsic factors like charged impurities and substrate ripples that limit the sample quality of graphene on conventional SiO_2 substrates [18]. This qualitative improvement in device qualities based on crystalline smooth barrier materials have led to the observation of new states of matter sensitive to disorder strength including new graphene fractional quantum Hall states [21,22], Fermi velocity renormalization [23], and anomalously large magnetodrag [24]. By forming different elementary combinations of both materials (see Fig. 1), we can obtain graphene on graphene (G/G), mainly in its Bernal [25–27] (AA stacking is metastable [28]) or twisted configuration [29,30], graphene on hexagonal boron nitride (G/BN) [31], and boron nitride on boron nitride (BN/BN) that can form moiré superlattices whenever there is a lattice constant mismatch or finite twist angle. Recent experimental [11,31,32] and theoretical works [12,33–37] have noted the relevance of moiré patterns and moiré strains in configuring the electronic structure near charge neutrality and at energy scales close to the superlattice Brillouin zones corners.

In this work we calculate the interlayer interactions through a calculation of distance and stacking-dependent energy differences that are required inputs to study the structural mechanics of the moiré strains in incommensurable crystals. This is a challenging task as the complex binding physics of layered van der Waals materials require theories that can explicitly account for the many-body effects [38,39]. We present an accurate parametrization of the interlayer coupling energies between layered materials consisting of graphene and hexagonal boron nitride vertical heterostructures, including their dependence on interlayer stacking configuration difference.

For high accuracy, total energies are calculated using high-level exact exchange and random phase approximation for the correlation energy (EXX+RPA or just RPA in short)

*jeiljung@uos.ac.kr

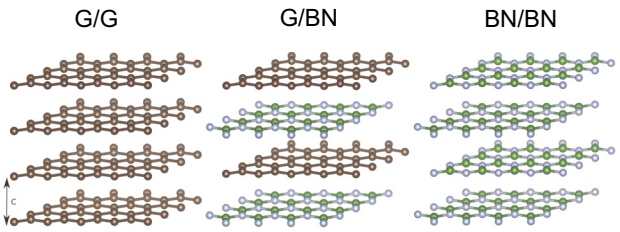

FIG. 1. Sketch of the three bulk systems considered in this paper. Here brown color corresponds to carbon forming graphene, while boron and nitrogen are gray and green, respectively. The interlayer spacing is represented by c. Two families of stacking configurations for 0° and 180° in an aligned BN/BN system, as explained in the main text and illustrated in Fig. 2.

ab initio calculations that are presented as a fitted correction to lower level local density approximation (LDA) calculations. The RPA is believed to be a good systematic approach to capture the total energy differences for graphite [40] and other layered systems [41]. We then use the fitted models to: (i) Show that the LDA can serve as a solid backbone to estimate such energy differences and associated force fields [42] at reasonable computational cost. We note that for G/BN the Lennard-Jones types of pairwise potentials can grossly underestimate the stacking-dependent energy barriers [43] by almost an order of magnitude with respect to *ab initio* approaches [13,44]. Therefore, our calculations can provide a more reliable input for molecular dynamic codes to study, for instance, the friction between such layered materials [45–49]. (ii) Improve qualitative predictions for equivalent bilayer systems, for sake of better experimental relevance. For this we use our fits to approximate high-level RPA data for bilayer systems, for which sufficiently accurate numerical RPA data are yet to be made available.

The rest of our article is structured as follows. Section II focuses on the details of the methodology, Sec. III discusses the results obtained for our different systems, while Sec. IV summarizes our findings.

II. METHODOLOGY AND COMPUTATIONAL DETAILS

The methodology we use to obtain the interlayer interaction for the different possible G/G, G/BN, BN/BN heterojunctions draws from the *ab initio* theory of moiré superlattices [12,13] for incommensurable crystals where the local interlayer interaction is modeled based on calculations performed for short period commensurate geometries. Similar earlier work attempting to capture interlayer interactions from different stacking geometries in commensurate G/BN were also presented in Refs. [33,44]. From information at a few selected stacking configurations obtained from small unit cell commensurate calculations we can build the energy landscape variations in the longer moiré pattern length scale for different interlayer separation distances. Here we revisit the calculations for G/G [40], BN/BN [41,50], and G/BN heterostructures [44,51,52], to analyze the stacking and interlayer distance dependent total energies in a consistent manner.

All calculations are carried out with the *ab initio* plane-wave code VASP [53] for bulk systems. For RPA correlation energy calculations, we use an $8 \times 8 \times 3$ Γ-centered k grid, an

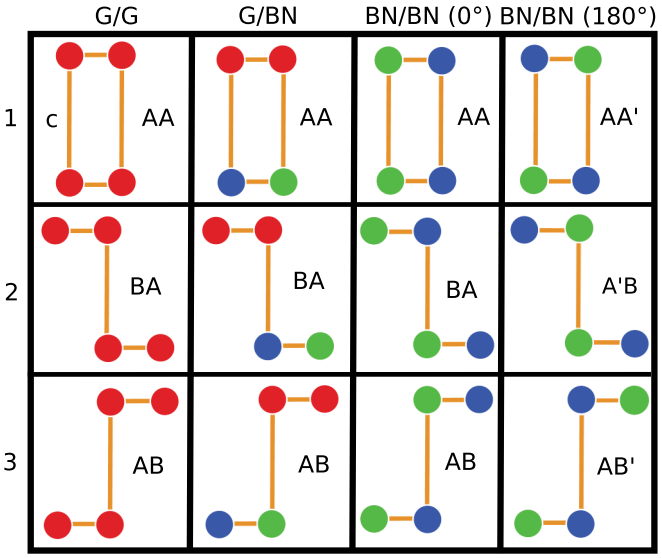

FIG. 2. Definition of stacking configurations $S = 1$, 2, or 3 for each system, in side view (top layer on top). Distance between layers is given by c. Carbon is red, boron is blue, and nitrogen is green. For G/BN we follow the definition in Ref. [12] where AB stacking denotes C on top of N ($a/\sqrt{3}$), while BA corresponds to C on top of B ($2a/\sqrt{3}$). For the other BN/BN configurations, we match naming conventions with the ones in Ref. [55]. By using the energies associated with each of these positions (or any other combination of three positions), one can extract the potential landscape of all stacking configurations.

energy cutoff of 700 eV, and a cutoff for the polarizability matrices of 300 eV. For the Hartree-Fock energy calculations that provides the exact-exchange (EXX) energies, we use the same energy cutoff but increase the k grid to $12 \times 12 \times 6$. The LDA calculations use an energy cutoff of 500 eV and a Γ-centered k grid of $16 \times 16 \times 8$. We use in-plane lattice parameters of 2.46 Å for graphene [40], 2.50 Å for BN [54], and their average 2.48 Å for the mixed G/BN system [44]. With these parameter choices, our results for bulk hexagonal BN in the lowest energy AA′ and AB configurations agree well with those found in previous work [41,50,55]. For example, for AA′, we find an interlayer distance of 3.36 versus 3.34 Å from Ref. [55]. For the binding energy of AB, we get 42 versus 39 meV/atom from Ref. [41]. Results for G/BN are also similar to bilayer calculations reported in Ref. [56].

To accurately interpolate the RPA results [57–59] as a function of interlayer separation distance c, we use the scheme suggested in Ref. [60]. We approximate RPA results by correcting LDA energies using

$$U_S^{\mathrm{RPA}}(c) \approx U_S^{\mathrm{LDA}}(c) + U_{\mathrm{Corr}}(c). \quad (1)$$

Here S denotes the chosen stacking configuration, see Fig. 2 for an illustration of the corresponding configurations.

This approach takes advantage of the good *short-range* accuracy of LDA DFT, but corrects its poor treatment of *long-range* effects using RPA results. By assuming that LDA is valid for distances below equilibrium separation where short-range covalent-binding dominates, and that the longer-range vdW dispersion potential takes the upper hand for distances beyond the equilibrium distance, we can separate both contributions

estimating the correction term by

$$U_{\rm Corr} = f(c)\big[U_{\rm vdW}(c) - U_S^{\rm LDA}(c)\big], \tag{2}$$

where

$$f(c) = \big[1 + \kappa_S \exp\big(-\big(a_1^S x_S + a_2^S x_S^2 + a_3^S x_S^3\big)\big)\big]^{-1}, \tag{3}$$

and use for the van der Waals tail description the function

$$U_{\rm vdW}(c) = -\frac{C_4}{(c^4 - D_s^4)} - \frac{C_3}{c^3}\frac{2}{\pi}\arctan\left(\frac{c}{D_C} + \phi_c\right) \tag{4}$$

for graphite to account for the interaction between the Dirac cones in G/G and for consistency with the asymptotic behavior in Ref. [60]. For all other systems when we have an insulating gap we use

$$U_{\rm vdW}(c) = -\frac{C_4}{\big(c^2 - D_s^2\big)^2}. \tag{5}$$

The LDA part is given by

$$U_S^{\rm LDA}(c) = -M_0^S\left[\frac{\tau_2^S e^{-\tau_1^S x_S^{\rm LDA}} - \tau_1^S e^{-\tau_2^S x_S^{\rm LDA}}}{\tau_2^S - \tau_1^S}\right], \tag{6}$$

where $x_S = c/c_{\rm RPA}^S - 1$ and $x_S^{\rm LDA} = c/c_{\rm LDA}^S - 1$. Equation (6) provides a fitting model for the LDA calculation of stacking S and simplifies to

$$U_S^{\rm LDA}(c) = -M_0^S\big(1 + \tau^S x_S^{\rm LDA}\big)e^{-\tau^S x_S^{\rm LDA}} \tag{7}$$

when $\tau_1^S = \tau_2^S = \tau^S$. This fitting approach allows us to closely compare the RPA results with LDA (or any other approximation) values as a function of different interlayer separation.

Furthermore, this fitting offers a second advantage. Due to the high computational cost for carrying out calculations for bilayer systems where a large vacuum is required, we can presently only obtain reliable RPA data for bulk systems. Using this fitting procedure it is possible to extract the parameters that approximate the behavior of bilayer systems using LDA calculations for bilayers and fitting again the parameters

TABLE I. Summary of numerical data based on the procedure outlined in Sec. II, as given by Eqs. (3)–(6). We differentiate between parameters that reproduce the LDA calculation, the vdW correction, and the fitting function f. The C_3 term exists only for systems with interactions between Dirac modes in different layers. For the bilayer systems we need to use a new set of LDA parameters to obtain the fits as well as modified $C_3^{\rm Bi}$, $C_4^{\rm Bi}$ parameters (see Appendix B for details). We list in the last two rows the optimal RPA bulk and (estimated) bilayer E_0 energies and associated interlayer distances as observables of interest. E_0 is obtained using $U_S^{\rm RPA}(c = c_S^{\rm RPA})$. The total energy values should be considered accurate to at best 1 meV/atom due to uncertainties related with methodological errors in the extrapolation and numerical convergence. The distances are accurate to around ±1%. We note that the interlayer distances $c_S^{\rm LDA}$ are different between the bulk and the bilayer systems, which we rationalize by the fact that a single layer in bulk is surrounded on both sides of the layer while for the bilayer the interface is only on one side. All energies are given in meV/atom and lengths are given in Angstroms.

		G/G			G/BN			BN/BN (180°)			BN/BN (0°)		
	Configuration (S)	AA	BA	AB	AA	BA	AB	AA′	AB′	A′B	AA	BA	AB
$\rm LDA_{Bulk}$	M_0^S	14.23	24.271	24.271	17.3	28.3	19.1	27.5	25.6	15.7	14.6	27.9	27.9
	$c_S^{\rm LDA}$	3.631	3.341	3.341	3.5	3.23	3.44	3.24	3.26	3.55	3.58	3.22	3.22
	τ_1^S	9.373	8.412	8.412	8.699	6.541	8.52	7.855	7.886	7.828	7.736	6.0	6.0
	τ_2^S	9.373	8.412	8.412	8.699	10.177	8.52	7.855	7.886	10.621	10.836	10.0	10.0
$\rm LDA_{Bi}$	M_0^S	9.664	13.312	13.312	8.232	14.110	9.155	13.832	12.500	7.622	7.090	13.809	13.809
	$c_S^{\rm LDA}$	3.557	3.32	3.32	3.535	3.216	3.457	3.24	3.3	3.56	3.6	3.25	3.25
	τ_1^S	8.645	7.837	7.838	8.181	7.569	8.058	7.827	8.399	9.356	8.610	8.123	8.123
	τ_2^S	8.645	7.837	7.838	8.181	7.569	8.059	7.827	8.399	9.356	8.610	8.124	8.124
f	κ_S	1.262	1.373	1.373	1.038	1.324	1.17	1.756	1.674	1.188	1.254	1.699	1.699
	a_1^S	6.843	11.496	11.496	10.8	12.7	11.1	13.5	14.0	12.3	12.0	14.2	14.2
	a_2^S	3.315	−5.586	−5.586	−11.8	−11.8	−9.8	−24.5	−35.0	−19.7	−3.8	−28.3	−28.3
	a_3^S	30.0	30.0	30.0	30.0	30.0	30.0	30.0	30.0	30.0	30.0	30.0	30.0
	$c_S^{\rm RPA}$	3.48	3.33	3.33	3.46	3.27	3.43	3.32	3.36	3.58	3.62	3.32	3.32
vdW	C_4		7570			7800			7100			7100	
	$C_4^{\rm Bi}$		3492.72			3603.6			3280.2			3280.2	
	D_S		2.22			0.86			0.86			0.86	
	C_3		380			0			0			0	
	$C_3^{\rm Bi}$		172.9			0			0			0	
	D_C		23.7			0			0			0	
	ϕ_c		0.62			0			0			0	
E_0	Bulk	−38	−49	−49	−39	−50	−40	−42	−39	−31	−29	−42	−42
	Bi	−19	−24	−24	−18	−23	−19	−20	−19	−14	−13	−20	−20

using the long-range correction terms estimated from the bulk behavior [60], see Appendix B for a more detailed discussion. This procedure is used to obtain the modified bilayer fitting parameters presented in Table I to obtain estimates for the total energy curves in bilayer geometries at RPA-level accuracy.

By calculating the bulk quantities for three stacking configurations, a general behavior of the interlayer binding energies can then be extrapolated for every case based on the approach outlined in Ref. [12]. The stacking-dependent energy landscape, in the first harmonic approximation, is given by

$$U(x,y,c) \approx C_0(c) + f_1(x,y,c,C_1,\phi_0), \tag{8}$$

where x, y are the in-plane stacking coordinates and c is the interlayer separation. The function f_1 follows from trigonal symmetry and is defined as

$$\begin{aligned} &f_1(x,y,c,C_1,\phi_0) \\ &\quad = 2C_1\cos(\phi_0 - G_1 y) + 4C_1\cos(G_1 y/2 + \phi_0) \\ &\qquad \times \cos(\sqrt{3}G_1 x/2), \end{aligned} \tag{9}$$

where C_0, C_1, and ϕ_0 are the three parameters to be fitted and $G_1 = 4\pi/\sqrt{3}a$ is the magnitude of the reciprocal lattice vector. In the case we have information of AA, AB, and BA stacking configurations these c dependent parameters can be written as follows [12]:

$$\phi(c) = \arctan\left[-\frac{\sqrt{3}}{2(D+1/2)}\right], \tag{10}$$

$$C_1(c) = \frac{U(0,2/\sqrt{3},c) - U(0,1/\sqrt{3},c)}{6\sqrt{3}\sin[\phi(c)]}, \tag{11}$$

and

$$C_0(c) = -6C_1\cos[\phi(c)] + U(0,0,c), \tag{12}$$

where

$$D = \frac{U(0,0,c) - U(0,1/\sqrt{3},c)}{U(0,1/\sqrt{3},c) - U(0,2/\sqrt{3},c)}. \tag{13}$$

We also derive more general expressions in Appendix A that allow us to combine *any* three stacking configurations to parametrize the in-plane potential landscape.

Finally, we calculate the interlayer elastic coefficient C_{33} and the interlayer inelastic coefficient C_{333} for the three stacking configurations of each system as defined in Ref. [60],

$$\frac{F_3(c)}{V_0} \approx C_{33}\left(\frac{c}{c_0} - 1\right) + \frac{1}{2}C_{333}\left(\frac{c}{c_0} - 1\right)^2, \tag{14}$$

where the normalized force per unit volume $F_3/V_0 \equiv (c/c_0)(dE/dc)$ depends on distortions in the out-of-plane direction through

$$C_{33} = \frac{c_0^2}{V_0}\frac{d^2E(c)}{dc^2}\bigg|_{c_0} \tag{15}$$

and

$$C_{333} = \frac{c_0^3}{V_0}\frac{d^3E(c)}{dc^3}\bigg|_{c_0}. \tag{16}$$

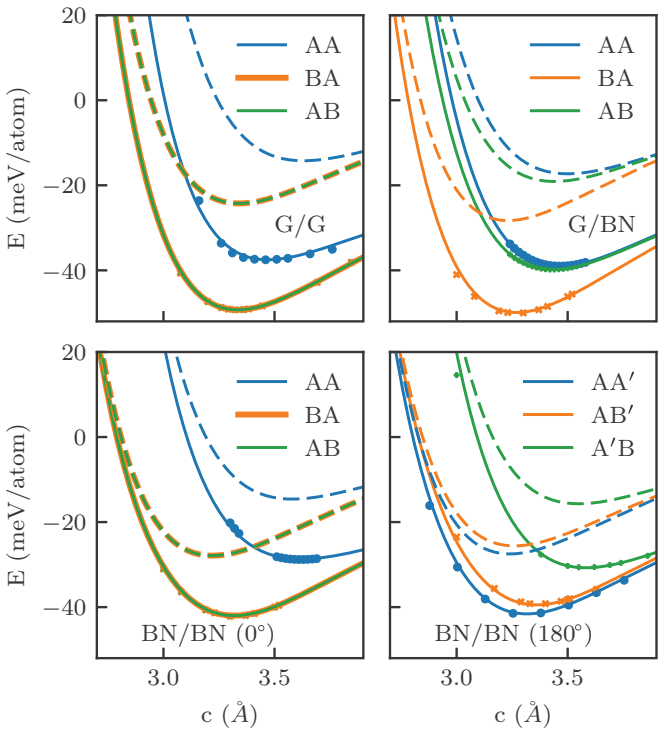

FIG. 3. Total energy from accurate bulk RPA and LDA calculations, as well as corresponding fitting lines based on Eqs. (1) to (7) for different stacking configurations for each system corresponding to parametrization given in Table I, as defined in Fig. 2. The symbols are calculated data points while the fits are represented as lines. The dashed lines are bulk LDA total energy fits. Our fitting procedure is particularly accurate in the region of interest where $c = 3$–4 Å.

III. RESULTS AND DISCUSSIONS

In this section we discuss the interlayer interaction energies obtained from the EXX+RPA calculations for the different G/G, G/BN, and BN/BN heterostructures considered. The fitting scheme for the interlayer energy curves based on Eqs. (1) to (7) are illustrated in Fig. 3 where we show the fitted curves in solid lines together with the data set represented by symbols for the different stacking configurations illustrated in Fig. 2. When we approximate the bilayer RPA behavior (see Table I) we obtain energies that are about twice as small as the bulk values (not shown here) consistent with the fact that there are fewer interfaces. The total energy values reported in this article should be considered accurate to at best 1 meV/atom due to uncertainties related with methodological errors in the extrapolation, and numerical convergence.

The pressure curves as a function of distance obtained by fitting the distance dependent energies with a Birch-Murnaghan equation of state [61] are shown in Fig. 4 for different stacking configurations. The results are provided both at the LDA (dashed lines) and RPA (solid lines) which show qualitative agreements in the ordering of the forces for the different stacking configurations although there are quantitative differences.

The energy landscapes based on Eq. (8) representing the total energies for different stacking at a fixed interlayer distance of $c = 3.4$ Å are shown in Fig. 5. Using a shared color map between the different systems it is possible to distinguish

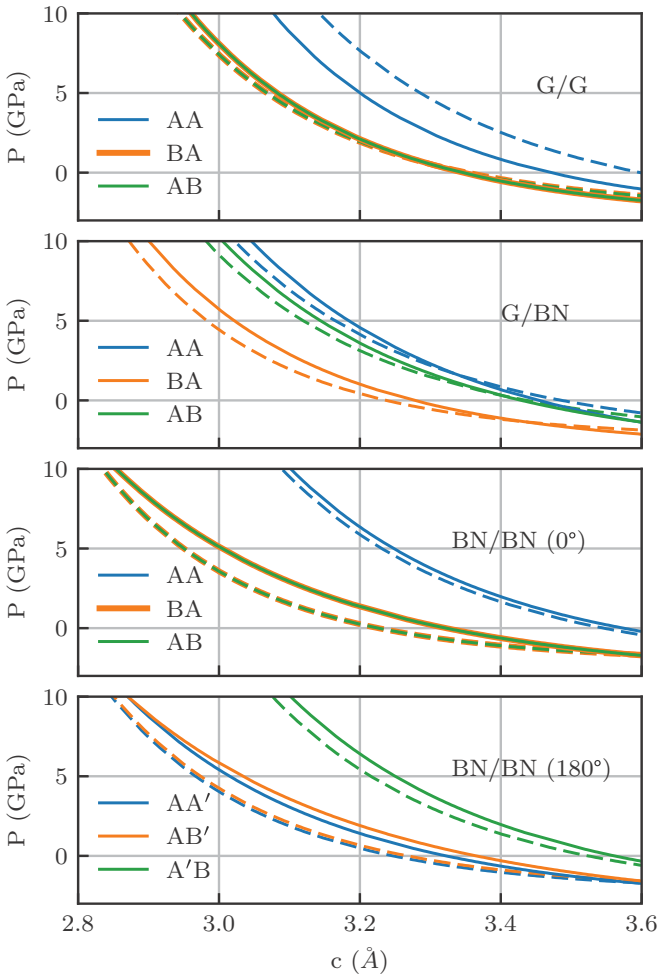

FIG. 4. Bulk equilibrium interlayer distance corresponding to different stacking positions as a function of pressure obtained at the RPA (solid) and LDA (dashed) level. The different colors represent the different stacking configurations that are defined in Fig. 3. The gradients of both approximations are very similar in the compression regime and have maximum deviations for the predicted equilibrium distances of ∼0.1 Å in the worst cases. Therefore, the LDA can be used as a reliable approximation for estimating the changes in interlayer distance with pressure.

the contrasts in the total energies, we see that, as expected, the less stable BN/BN (0°) system produces the largest energy variations between different stackings (up to ∼16 meV/atom), opposing smooth sliding between the layers and potentially enhancing in-plane moiré strains. The other systems have comparatively smaller maximum energy differences: G/BN is lowest with ∼10 meV/atom while BN/BN (180°) and G/G systems generate values of about 13 and 12 meV/atom, respectively. In Fig. 6 we plot the parameters $C_0(c)$, $C_1(c)$, and $\phi(c)$ that control this stacking dependent energy landscapes, as given by Eqs. (10) to (12) for each system. The $C_0(c)$ is the average stacking dependent total energy at a given interlayer separation c, whereas $C_1(c)$ and $\phi(c)$ are the magnitude and phase of the stacking dependent energy modulation described within the first harmonics. The magnitude represents the amplitude of the oscillation while the phase indicates the degree of mixing between inversion symmetric and inversion asymmetric contributions to the moire pattern modulations [62]. The lower-right 2×2 panel gives the vertical cut at $x = 0$ of the energy landscape for both LDA and RPA approximations and their differences. An overview of all the numerical data based on this procedure outlined in Sec. II is provided in Table I.

Finally, the interlayer elastic and inelastic coefficients, given by Eqs. (15) and (16), calculated at the equilibrium separation c_0 are summarized in Table II.

In the following we discuss in some detail the interlayer interaction properties of the different systems consisting of G/G, G/BN, and the two different BN/BN stacking configurations.

A. G/G

The interlayer binding energy of bilayer graphene can be understood as the elementary cohesive energy between the layers in graphite. The cleavage energy, approximately equal to the binding energy, of graphite has been measured based on the self-retraction phenomenon in graphite [63,64], while computationally the cohesive energies have been calculated in the past at different levels of approximation [65–70], and more recently through accurate RPA calculations carried out on graphite [40] that allowed us to confirm the weak nonadditivity effects due to long-range van der Waals interactions. Within RPA the binding energies at the equilibrium distance are equal to 49 meV/atom at Bernal stacking and 38 meV/atom for the least stable AA stacking (see Fig. 3), while for intermediate stacking configurations the binding energies vary between these two values as shown in Fig. 5.

The elastic and inelastic coefficients listed in Table II (also for AA stacking, extending the available data for Bernal stacking [60]) are significantly enhanced (up to 40%) when the long-range interactions are included within RPA compared to the LDA. For the bilayer coefficients one obtains values that are of the same order of magnitude as the bulk when we multiply the results by two (we do not report the inelastic coefficients of bilayer RPA, as the results are only approximate and we cannot benchmark it against directly calculated RPA data yet). This factor two multiplication is required to make a comparison with the bulk as there are twice as many interlayer neighbors in the latter case.

The energy profile for G/G resulting from the fitting parameters are plotted in Fig. 6. The C_0 corresponds to the average between the energies at the AA, AB, and BA stacking, while the binding energy equal to 44 meV/atom is a value that is more than doubled when compared to the LDA. The differences between the energy average and the minimum is approximately 4 meV/atom and indicates the order of magnitude for the energy gradient that controls the in-plane forces [12]. The relatively flat green curve (based on the difference between RPA and the LDA absolute energy data) in the lower-right panel of the figure illustrates that LDA yields accurate predictions on energy differences for this system that are fairly close to the RPA results.

B. G/BN

When we calculate the total energies for graphene and BN heterojunctions, we ignore the ∼2% lattice constant

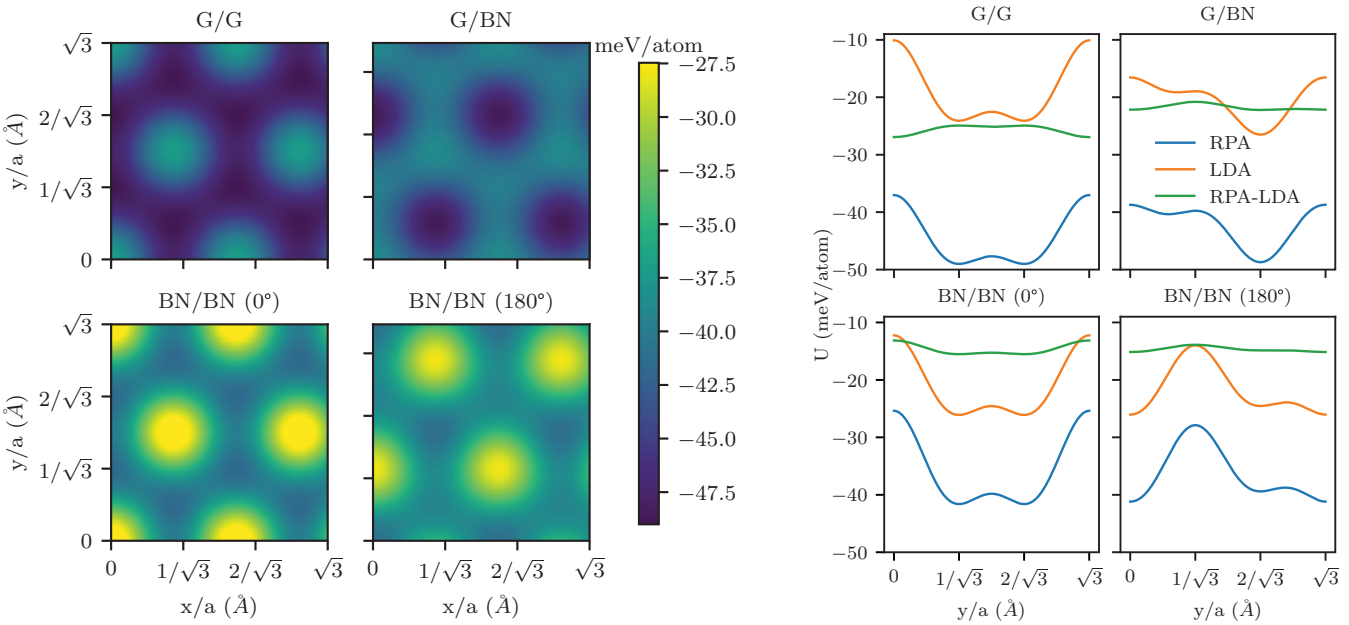

FIG. 5. *Left panel:* Two-dimensional maps of energy landscapes given by Eq. (8) for the RPA fits, for $c = 3.4$ Å. The parameters building these fits are in turn represented in Fig. 6, as well as a cut of the energy map along the $x = 0$ axis. The energy differences are largest for the BN/BN (60°) system of nonalternating atoms between layers, suggesting larger lattice reconstruction than for the other systems. *Right panel:* The vertical cut at $x = 0$ of the energy landscape (at an interlayer distance of 3.4 Å) for both LDA (orange) and RPA (blue) approximations, as well as their respective difference (green curve). The nearly constant behavior of the latter supports the main message of the paper, namely that the LDA yields accurate predictions for any type of quantity that takes energy differences as input variable. For the G/BN and BN/BN (0°) system, the y coordinates of AB (BA) stacking correspond to $a/\sqrt{3}$ ($2a/\sqrt{3}$), respectively, where a is the lattice constant of the unit cell. For the BN/BN (180°) system, the y coordinates of A′B (AB′) stacking correspond to $a/\sqrt{3}$ ($2a/\sqrt{3}$), respectively.

mismatch and obtain the interlayer stacking-dependent total energies as in Ref. [44] using an averaged lattice constant of $a = 2.48$ Å. These stacking dependent total energies based on LDA calculations were useful references for identifying the role of spontaneous strains in G/BN heterojunctions giving rise to a band gap [12]. The fitted RPA results for different stacking and interlayer distances are plotted in Fig. 6 where the green curve in the lower right panel validates the use of LDA data to estimate the stacking-dependent energy differences and associated strains in Ref. [12]. The total energy difference between the least favorable AA and most favorable BA stacking configuration is of the order of 10 meV/atom and is comparable to the LDA results, as well as the stacking dependent total energy differences in G/G. Our binding energy of 23 meV/atom estimated from bulk is in fair agreement with the direct calculation of 21 meV/atom in the isolated bilayer geometry in Ref. [44].

When we calculate and compare the interlayer elastic and inelastic coefficients, we observe, similarly to the G/G system, a drastic enhancement when including long-range corrections as compared to the LDA calculations, up to 40% for bilayer AA stacking and therefore the use of the RPA data is required to properly estimate these constants. The largest elastic coefficients are obtained at the most stable BA structure that corresponds to the situation where one carbon atom is on top of boron.

TABLE II. Summary of the interlayer elastic C_{33} and inelastic C_{333} coefficients as defined in Eqs. (15) and (16), in GPa, comparing values obtained within LDA and RPA, for bulk and bilayer systems. The C_{333} values are not listed for bilayers because we have not carried out direct bilayer RPA calculations. The stacking configurations 1, 2, and 3 are represented in Fig. 2. The relevance of long-range correlations is partly manifested in the impact made on these constants by the RPA.

	G/G			G/BN			BN/BN (180°)			BN/BN (0°)		
Configuration (S)	AA	BA	AB	AA	BA	AB	AA′	AB′	A′B	AA	BA	AB
C_{33}^{RPA}	29	37	37	32	38	30	32	32	24	18	31	31
C_{333}^{RPA}	−580	−600	−600	−560	−570	−500	−420	−370	−430	−360	−370	−370
C_{33}^{LDA}	21	31	31	23	35	24	31	29	21	20	31	31
C_{333}^{LDA}	−400	−520	−520	−400	−580	−420	−480	−450	−400	−370	−490	−490
$C_{33}^{\mathrm{RPA,Bi}}$	17	18	18	15	18	14	16	18	16	10	17	17
$C_{33}^{\mathrm{LDA,Bi}}$	12	15	15	9	15	10	16	16	11	9	17	17

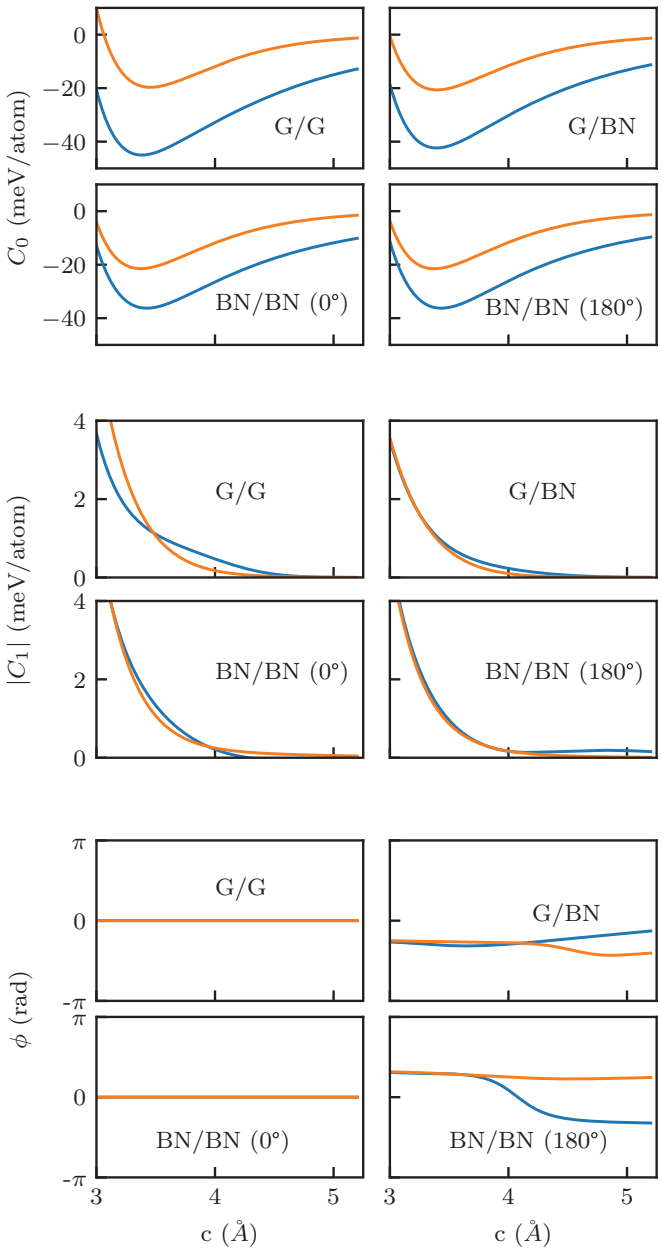

FIG. 6. The parameters in Eqs. (10)–(12) the $C_0(c)$ captures the average stacking dependent total energy at a given interlayer separation c, $C_1(c)$ is the first Fourier component magnitude and $\phi(c)$ is the phase associated with the stacking dependent energy modulation landscape given in the LDA (orange) and RPA (blue) approximations for each one of the systems considered.

C. BN/BN

Hexagonal boron nitride layers share many similar aspects to the bilayer graphene while the most notable difference is the polar character of their interatomic bonds and the marked distinction between each atom species within each layer. Due to their ionic character, the most stable crystalline form in their hexagonal geometry is the vertically alternating arrangement of the atoms in the AA′-stacking configuration (in our figures and table referred to as BN/BN 180°). We also provide data for the case with nonalternating atoms (BN/BN 0°). We note that according to our RPA data the AB configuration is nearly as stable as the AA′ one (less than 1 meV/atom), thus explaining the existence of both configurations in experiment [71].

The resulting fitting parameters for these BN/BN systems are plotted in Fig. 6 and confirm our main conclusions regarding the qualitative validity of LDA data. We further note that the BN/BN systems give larger values of C_1, indicating that these systems will have a stronger tendency to lock into an energetically more stable stacking configuration.

Unlike the G/G and G/BN systems, in BN/BN systems the LDA and RPA predict similar interlayer elastic and inelastic coefficients, perhaps reflecting a greater role of ionic effects that are well captured by LDA. Nevertheless, small changes are still observed and one should resort to RPA data whenever available.

IV. SUMMARY AND DISCUSSIONS

We have presented an accurate parametrization of the van der Waals interaction energies in 2D artificial materials that can be formed using graphene and hexagonal boron nitride single layers. Our methodology based on the RPA density-density response function is able to capture from first principles the many-body nonlocal Coulomb correlation effects that are responsible for a large part of interlayer binding.

The benchmark against our first-principles EXX+RPA calculation suggests that the success of the LDA in calculating the equilibrium geometries in the systems we considered for different stacking can be traced to its ability for capturing reliably the electronic structure in the covalent regime where the interatomic repulsion is important, and to a fortuitous tendency to overbind the layers at a moderately large interlayer separation distance. The LDA can thus be considered an accurate first approximation to predict friction energies in the layered materials considered.

We note that advances for methods beyond the LDA have already been made [51] using implementations by Tkatchenko-Scheffler and many-body dispersion methods [72,73] to account for the dispersion forces. However, despite ongoing improvements [74] in the semiempirical treatment of dispersion forces in layered systems, the RPA still provides a superior theoretical framework for making predictions of the interlayer interactions over the explored length scales, albeit at greater computational cost. Since the LDA fails to describe long-range interactions it should be corrected, whenever possible, to incorporate these effects when calculating the interlayer elastic and inelastic coefficients, as demonstrated in this work.

This procedure to assess and improve the qualitative role of the LDA can be applied routinely to a variety of layered 2D materials. Here we have used the approach to approximate RPA-level calculations for bilayers, that allows us to make reliable predictions for interlayer geometries. In order to go beyond the RPA one should consider short-range correlations by modeling the exchange-correlation kernel that can incorporate the many-body effects in a more precise manner [75–78].

ACKNOWLEDGMENTS

This work has been supported by the Korean NRF under Grant No. NRF-2015K2A1B8066011 and the Korea Research

Fellowship Program through the NRF funded by the Ministry of Science and ICT (NRF-2016H1D3A1023826). T.G. acknowledges support of the Griffith University Gowonda HPC Cluster.

APPENDIX A: PARAMETRIZATION OF THE POTENTIAL ENERGY

In the main text we provide the simple expressions that allow us to extract the potential landscape from the energies at AA, AB, and BA stacking. Here we give the more general expressions that allow us to extract the information from the combination of *any* three stacking configurations. We omit the c dependence to simplify the notation. After some algebra on Eq. (9), using the energies of three arbitrary configurations that are given by their respective coordinates

$$A = \phi(A_x, A_y), \tag{A1}$$

$$B = \phi(B_x, B_y), \tag{A2}$$

$$C = \phi(C_x, C_y), \tag{A3}$$

one finds that

$$\phi = \arctan\left[\frac{1}{\frac{\delta}{\beta}D - 1}\frac{\delta\alpha - \beta\gamma}{\beta\delta} - \frac{\gamma}{\delta}\right], \tag{A4}$$

$$C_1 = \frac{B - C}{2(\gamma\cos\phi + \delta\sin\phi)}, \tag{A5}$$

and

$$C_0 = A - 2C_1\cos(\phi - G_1A_y) - 4C_1\cos(G_1A_y/2 + \phi) \times \cos(\sqrt{3}G_1A_x/2), \tag{A6}$$

where

$$\alpha = a_1 + a_3, \tag{A7}$$

$$\beta = a_2 - a_4, \tag{A8}$$

$$\gamma = b_1 + b_3, \tag{A9}$$

$$\delta = b_2 - b_4, \tag{A10}$$

$$D = \frac{A - B}{B - C}, \tag{A11}$$

with

$$a_1 = \cos(G_1A_y) - \cos(G_1B_y), \tag{A12}$$

$$a_2 = \sin(G_1A_y) - \sin(G_1B_y), \tag{A13}$$

$$a_3 = 2\cos(G_1A_y/2)m_A - 2\cos(G_1B_y/2)m_B, \tag{A14}$$

$$a_4 = 2\sin(G_1A_y/2)m_A - 2\sin(G_1B_y/2)m_B, \tag{A15}$$

$$b_1 = \cos(G_1B_y) - \cos(G_1C_y), \tag{A16}$$

$$b_2 = \sin(G_1B_y) - \sin(G_1C_y), \tag{A17}$$

$$b_3 = 2\cos(G_1B_y/2)m_B - 2\cos(G_1C_y/2)m_C, \tag{A18}$$

$$b_4 = 2\sin(G_1B_y/2)m_B - 2\sin(G_1C_y/2)m_C, \tag{A19}$$

and finally

$$m_A = \cos(\sqrt{3}G_1A_x/2), \tag{A20}$$

$$m_B = \cos(\sqrt{3}G_1B_x/2), \tag{A21}$$

$$m_C = \cos(\sqrt{3}G_1C_x/2). \tag{A22}$$

These expressions have been cross checked with the simpler expressions derived previously [12], and are valid for any system that possesses trigonal symmetry, as is the case of many layered materials not considered here.

APPENDIX B: BILAYER FITTING EXPRESSIONS

The vdW dispersion and the LDA fits for bilayer systems are similar to the expressions in Eqs. (4)–(6):

$$U_{\mathrm{vdW,Bi}}(c) = -\frac{C_4^{\mathrm{Bi}}}{\left(c^2 - D_s^{\mathrm{Bi}^2}\right)^2} - \frac{C_3^{\mathrm{Bi}}}{c^3}\frac{2}{\pi}\arctan\left(\frac{c}{D_C^{\mathrm{Bi}}} + \phi_c^{\mathrm{Bi}}\right), \tag{B1}$$

$$U_S^{\mathrm{LDA,Bi}}(c) = -M_0^{S,\mathrm{Bi}} \times\left[\frac{\tau_2^{S,\mathrm{Bi}}e^{-\tau_1^{S,\mathrm{Bi}}x_S^{\mathrm{LDA}}} - \tau_1^{S,\mathrm{Bi}}e^{-\tau_2^{S,\mathrm{Bi}}x_S^{\mathrm{LDA}}}}{\tau_2^{S,\mathrm{Bi}} - \tau_1^{S,\mathrm{Bi}}}\right], \tag{B2}$$

with a different set of parameters than the ones obtained for the bulk. Similar to the bulk, the C_3^{Bi} term is nonzero for graphene only. Some of us have argued previously [60] that the most important changes occur to the parameters C_3^{Bi}, C_4^{Bi}, and $M_0^{S,\mathrm{Bi}}$ and those are the only ones that have to be rescaled. The method to obtain these scaling factors for bilayer graphene is outlined in Ref. [60], and are respectively given by 0.455, 0.462, and 0.5. The latter was obtained assuming $U^{\mathrm{LDA,Bi}} = \frac{1}{2}U^{\mathrm{LDA}}$.

Here we perform the bilayer LDA calculations for all systems, and confirm that the assumption on M_0 is reasonable as a first approximation. However, some of the G/G bulk structures can, comparatively, become even more stable in their bilayer form, while the opposite behavior is generally true for the other systems. Due to the fact that a bilayer has only one interface there are changes in the interlayer equilibrium distances with respect to bulk. In Table I the results for bilayer have thus been obtained by directly fitting bilayer LDA data using Eq. (B2).

[1] A. Koma, Thin Solid Films **216**, 72 (1992).

[2] A. Koma, J. Cryst. Growth **201-202**, 236 (1999).

[3] A. K. Geim and I. V. Grigorieva, Nature (London) **499**, 419 (2013).

[4] K. S. Novoselov, D. Jiang, F. Schedin, T. J. Booth, V. V. Khotkevich, S. V. Morozov, and A. K. Geim, Proc. Nat. Acad. Sci. USA **102**, 10451 (2005).

[5] K. S. Novoselov, A. K. Geim, S. V. Morozov, D. Jiang, M. I. Katsnelson, I. V. Grigorieva, S. V. Dubonos, and A. A. Firsov, Nature (London) **438**, 197 (2005).

[6] Y. Zhang, Y.-W. Tan, H. L. Stormer, and P. Kim, Nature (London) **438**, 201 (2005).

[7] C. R. Dean, L. Wang, P. Maher, C. Forsythe, F. Ghahari, Y. Gao, J. Katoch, M. Ishigami, P. Moon, M. Koshino, T. Taniguchi, K. Watanabe, K. L. Shepard, J. Hone, and P. Kim, Nature (London) **497**, 598 (2013).

[8] L. A. Ponomarenko, R. V. Gorbachev, G. L. Yu, D. C. Elias, R. Jalil, A. A. Patel, A. Mishchenko, A. S. Mayorov, C. R. Woods, J. R. Wallbank, M. Mucha-Kruczynski, B. A. Piot, M. Potemski, I. V. Grigorieva, K. S. Novoselov, F. Guinea, V. I. Fal'ko, and A. K. Geim, Nature (London) **497**, 594 (2013).

[9] J. S. Alden, A. W. Tsen, P. Y. Huang, R. Hovden, L. Brown, J. Park, D. A. Muller, and P. L. McEuen, Proc. Natl. Acad. Sci. USA **110**, 11256 (2013).

[10] B. Butz, C. Dolle, F. Niekiel, K. Weber, D. Waldmann, H. B. Weber, B. Meyer, and E. Spiecker, Nature (London) **505**, 533 (2013).

[11] C. R. Woods, L. Britnell, A. Eckmann, R. S. Ma, J. C. Lu, H. M. Guo, X. Lin, G. L. Yu, Y. Cao, R. V. Gorbachev, A. V. Kretinin, J. Park, L. A. Ponomarenko, M. I. Katsnelson, Y. N. Gornostyrev, K. Watanabe, T. Taniguchi, C. Casiraghi, H.-J. Gao, A. K. Geim, and K. S. Novoselov, Nat. Phys. **10**, 451 (2014).

[12] J. Jung, A. M. DaSilva, A. H. MacDonald, and S. Adam, Nat. Commun. **6**, 6308 (2015).

[13] J. Jung, A. Raoux, Z. Qiao, and A. H. MacDonald, Phys. Rev. B **89**, 205414 (2014).

[14] A. K. Geim and K. S. Novoselov, Nat. Mater. **6**, 183 (2007).

[15] S. Das Sarma, S. Adam, E. H. Hwang, and E. Rossi, Rev. Mod. Phys. **83**, 407 (2011).

[16] A. K. Geim and A. H. MacDonald, Phys. Today **60**(8), 35 (2007).

[17] A. H. Castro Neto, F. Guinea, N. M. R. Peres, K. S. Novoselov, and A. K. Geim, Rev. Mod. Phys. **81**, 109 (2009).

[18] C. R. Dean, A. F. Young, I. Meric, C. Lee, L. Wang, S. Sorgenfrei, K. Watanabe, T. Taniguchi, P. Kim, K. L. Shepard, and J. Hone, Nat. Nanotechnol. **5**, 722 (2010).

[19] A. Zunger, A. Katzir, and A. Halperin, Phys. Rev. B **13**, 5560 (1976).

[20] G. W. Semenoff, Phys. Rev. Lett. **53**, 2449 (1984).

[21] X. Du, I. Skachko, F. Duerr, A. Luican, and E. Y. Andrei, Nature (London) **462**, 192 (2009).

[22] K. I. Bolotin, F. Ghahari, M. D. Shulman, H. L. Stormer, and P. Kim, Nature (London) **462**, 196 (2009).

[23] D. C. Elias, R. V. Gorbachev, A. S. Mayorov, S. V. Morozov, A. A. Zhukov, P. Blake, L. A. Ponomarenko, I. V. Grigorieva, K. S. Novoselov, F. Guinea, and A. K. Geim, Nat. Phys. **7**, 701 (2011).

[24] R. V. Gorbachev, A. K. Geim, M. I. Katsnelson, K. S. Novoselov, T. Tudorovskiy, I. V. Grigorieva, A. H. MacDonald, S. V. Morozov, K. Watanabe, T. Taniguchi, and L. A. Ponomarenko, Nat. Phys. **8**, 896 (2012).

[25] K. Yan, H. Peng, Y. Zhou, H. Li, and Z. Liu, Nano Lett. **11**, 1106 (2011).

[26] K. Kim, M. Yankowitz, B. Fallahazad, S. Kang, H. C. P. Movva, S. Huang, S. Larentis, C. M. Corbet, T. Taniguchi, K. Watanabe, S. K. Banerjee, B. J. LeRoy, and E. Tutuc, Nano Lett. **16**, 1989 (2016).

[27] J. Lin, W. Fang, W. Zhou, A. R. Lupini, J. C. Idrobo, J. Kong, S. J. Pennycook, and S. T. Pantelides, Nano Lett. **13**, 3262 (2013).

[28] P. L. de Andres, R. Ramírez, and J. A. Vergés, Phys. Rev. B **77**, 045403 (2008).

[29] L. Brown, R. Hovden, P. Huang, M. Wojcik, D. A. Muller, and J. Park, Nano Lett. **12**, 1609 (2012).

[30] J. Park, W. C. Mitchel, S. Elhamri, L. Grazulis, J. Hoelscher, K. Mahalingam, C. Hwang, S.-K. Mo, and J. Lee, Nat. Commun. **6**, 5677 (2015).

[31] M. Yankowitz, J. Xue, D. Cormode, J. D. Sanchez-Yamagishi, K. Watanabe, T. Taniguchi, P. Jarillo-Herrero, P. Jacquod, and B. J. LeRoy, Nat. Phys. **8**, 382 (2012).

[32] B. Hunt, J. D. Sanchez-Yamagishi, A. F. Young, M. Yankowitz, B. J. LeRoy, K. Watanabe, T. Taniguchi, P. Moon, M. Koshino, P. Jarillo-Herrero, and R. C. Ashoori, Science **340**, 1427 (2013).

[33] G. Giovannetti, P. A. Khomyakov, G. Brocks, P. J. Kelly, and J. van den Brink, Phys. Rev. B **76**, 073103 (2007).

[34] J. M. B. Lopes dos Santos, N. M. R. Peres, and A. H. Castro Neto, Phys. Rev. Lett. **99**, 256802 (2007).

[35] J. M. B. Lopes dos Santos, N. M. R. Peres, and A. H. Castro Neto, Phys. Rev. B **86**, 155449 (2012).

[36] R. Bistritzer and A. H. MacDonald, Proc. Natl. Acad. Sci. USA **108**, 12233 (2011).

[37] J. R. Wallbank, A. A. Patel, M. Mucha-Kruczyński, A. K. Geim, and V. I. Fal'ko, Phys. Rev. B **87**, 245408 (2013).

[38] J. F. Dobson and T. Gould, J. Phys.: Condens. Matter **24**, 073201 (2012).

[39] T. Gould, S. Lebègue, T. Björkman, and J. Dobson, in *2D Materials*, Semiconductors and Semimetals, Vol. 95, edited by J. J. B. Francesca Iacopi and C. Jagadish (Elsevier, Amsterdam, 2016), pp. 1–33.

[40] S. Lebègue, J. Harl, T. Gould, J. G. Ángyán, G. Kresse, and J. F. Dobson, Phys. Rev. Lett. **105**, 196401 (2010).

[41] T. Björkman, A. Gulans, A. V. Krasheninnikov, and R. M. Nieminen, J. Phys.: Condens. Matter **24**, 424218 (2012).

[42] I. Leven, I. Azuri, L. Kronik, and O. Hod, J. Chem. Phys. **140**, 104106 (2014).

[43] M. Neek-Amal and F. M. Peeters, Appl. Phys. Lett. **104**, 041909 (2014).

[44] B. Sachs, T. O. Wehling, M. I. Katsnelson, and A. I. Lichtenstein, Phys. Rev. B **84**, 195414 (2011).

[45] M. M. van Wijk, M. Dienwiebel, J. W. M. Frenken, and A. Fasolino, Phys. Rev. B **88**, 235423 (2013).

[46] M. Reguzzoni, A. Fasolino, E. Molinari, and M. C. Righi, J. Phys. Chem. C **116**, 21104 (2012).

[47] A. L. Kitt, Z. Qi, S. Rémi, H. S. Park, A. K. Swan, and B. B. Goldberg, Nano Lett. **13**, 2605 (2013).

[48] M. Reguzzoni, A. Fasolino, E. Molinari, and M. C. Righi, Phys. Rev. B **86**, 245434 (2012).

[49] S. G. Balakrishna, A. S. de Wijn, and R. Bennewitz, Phys. Rev. B **89**, 245440 (2014).

[50] A. Marini, P. García-González, and A. Rubio, Phys. Rev. Lett. **96**, 136404 (2006).

[51] I. Leven, T. Maaravi, I. Azuri, L. Kronik, and O. Hod, J. Chem. Theory Comput. **12**, 2896 (2016).

[52] K. Thürmer and C. D. Spataru, Phys. Rev. B **95**, 035432 (2017).

[53] G. Kresse and J. Furthmüller, Phys. Rev. B **54**, 11169 (1996).
[54] R. S. Pease, Acta Crystallogr. **5**, 356 (1952).
[55] G. Constantinescu, A. Kuc, and T. Heine, Phys. Rev. Lett. **111**, 036104 (2013).
[56] S. Zhou, J. Han, S. Dai, J. Sun, and D. J. Srolovitz, Phys. Rev. B **92**, 155438 (2015).
[57] O. Gunnarsson and B. I. Lundqvist, Phys. Rev. B **13**, 4274 (1976).
[58] D. C. Langreth and J. P. Perdew, Phys. Rev. B **15**, 2884 (1977).
[59] D. Langreth and J. Perdew, Solid State Commun. **17**, 1425 (1975).
[60] T. Gould, S. Lebègue, and J. F. Dobson, J. Phys.: Condens. Matter **25**, 445010 (2013).
[61] F. Birch, Phys. Rev. **71**, 809 (1947).
[62] J. Jung, E. Laksono, A. M. DaSilva, A. H. MacDonald, M. Mucha-Kruczynski, and S. Adam, Phys. Rev. B **96**, 085442 (2017).
[63] W. Wang, S. Dai, X. Li, J. Yang, D. J. Srolovitz, and Q. Zheng, Nat. Commun. **6**, 7853 (2015).
[64] Q. Zheng, B. Jiang, S. Liu, Y. Weng, L. Lu, Q. Xue, J. Zhu, Q. Jiang, S. Wang, and L. Peng, Phys. Rev. Lett. **100**, 067205 (2008).
[65] S. Grimme, J. Comput. Chem. **27**, 1787 (2006).
[66] K. Lee, E. D. Murray, L. Kong, B. I. Lundqvist, and D. C. Langreth, Phys. Rev. B **82**, 081101 (2010).
[67] J. Sun, R. Haunschild, B. Xiao, I. W. Bulik, G. E. Scuseria, and J. P. Perdew, J. Chem. Phys. **138**, 044113 (2013).
[68] D. C. Langreth and J. P. Perdew, Phys. Rev. B **21**, 5469 (1980).
[69] S. Sorella, M. Casula, and D. Rocca, J. Chem. Phys. **127**, 014105 (2007).
[70] N. D. Drummond and R. J. Needs, Phys. Rev. Lett. **99**, 166401 (2007).
[71] J. H. Warner, M. H. Rümmeli, A. Bachmatiuk, and B. Büchner, ACS Nano **4**, 1299 (2010).
[72] A. Tkatchenko and M. Scheffler, Phys. Rev. Lett. **102**, 073005 (2009).
[73] A. Tkatchenko, R. A. DiStasio, Jr., R. Car, and M. Scheffler, Phys. Rev. Lett. **108**, 236402 (2012).
[74] T. Gould, S. Lebègue, J. G. Ángyán, and T. Bucko, J. Chem. Theory Comput. **12**, 5920 (2016).
[75] T. Olsen and K. S. Thygesen, Phys. Rev. B **86**, 081103 (2012).
[76] T. Gould, J. Chem. Phys. **137**, 111101 (2012).
[77] J. F. Dobson, T. Gould, and G. Vignale, Phys. Rev. X **4**, 021040 (2014).
[78] J. Jung, P. García-González, J. F. Dobson, and R. W. Godby, Phys. Rev. B **70**, 205107 (2004).